Available online at www.sciencedirect.com

ScienceDirect

Energy Procedia 114 (2017) 446 – 457

Energy Procedia

13th International Conference on Greenhouse Gas Control Technologies, GHGT-13, 14-18 November 2016, Lausanne, Switzerland

The internally circulating reactor (ICR) concept applied to pressurized chemical looping processes

Schalk Cloete, Abdelghafour Zaabout & Shahriar Amini

Flow Technology Group, SINTEF Materials and Chemistry, S.P. Andersens vei 15B, 7031 Trondheim, Norway

Abstract

The internally circulating reactor (ICR) has significant potential to reduce costs and simplify scale-up of pressurized chemical looping process concepts. An ICR consists of a single reactor body divided into two or three sections where different reactions are carried out. Simple ports connect the reactor sections to ensure circulation of the oxygen carrier. The cost of this simplicity is a certain amount of gas leakage between reactor sections. Quantification of this leakage revealed good CO_2 purity and capture (>96%) for combustion, reforming and oxygen production chemical looping applications, but poorer CO_2 separation performance for water splitting.

Peer-review under responsibility of the organizing committee of GHGT-13.

Keywords: Internally circulating reactor; Chemical looping combustion; Chemical looping reforming; Chemical looping oxygen production; Chemical looping water splitting; Dense discrete phase model; CO_2 capture

1. Introduction

Chemical looping has arisen as a promising technology with great potential to reduce the costs associated with clean utilization of fossil fuels. It was first applied to combustion through the CLC process [1, 2], where inherent separation of CO_2 and N_2 is ensured, using an oxygen carrier circulating between two reactors, namely air and fuel reactors, transferring oxygen from air to fuel. The low energy penalty of CLC relative to other CO_2 capture technologies has led to extensions of the chemical looping principle to other CO_2 and energy intensive processes such as reforming [3], air separation [4] and hydrogen generation through the steam-iron process [5].

High-pressure operation of these chemical looping concepts is necessary for maximizing energy efficiency and competitiveness with other CO_2 capture technologies, but upscaling of pressurized chemical looping processes has been slow. This is due to the challenges linked to the use of the interconnected reactor configuration involving external solids separation; to the authors' knowledge, only one study on pressurized CLC in interconnected fluidized

Peer-review under responsibility of the organizing committee of GHGT-13.
doi:10.1016/j.egypro.2017.03.1187

beds has been completed to date [6]. This limitation has prompted research into novel reactor concepts to improve the scalability of pressurized chemical looping technology.

Several reactor concepts have been proposed to avoid external solids circulation to remove scale-up issues under pressurized operation. This includes Gas Switching concepts based on packed and fluidized beds [7, 8], and the internally circulating reactor (ICR) which is the subject of this paper [9]. The ICR concept (Figure 1) uses a single reactor divided into two chambers with two connecting ports, one in the top and the other in the bottom. The two chambers are fluidized at different gas flow rates and the solids in the chamber with the larger flow rate are transported to the freeboard to fall and circulate into the second chamber through the port in the top. Accumulation of solids in the second chamber creates a pressure difference between the two sides of the port at the bottom, which provides a driving force for solids circulation back to the first chamber.

The simplicity of the ICR comes at the expenses of gas leakage, which takes place between the two chambers through the connecting ports. A cold flow model of the ICR reactor was therefore designed and constructed in order to investigate the gas leakage [9]. It was shown that gas leakage could be maintained at acceptable levels over a relatively wide range of operating conditions and it was concluded that the ICR is well suited for chemical looping processes. This work will further build on this initial study by simulating a large-scale ICR and assessing CO_2 separation performance for four different chemical looping technologies.

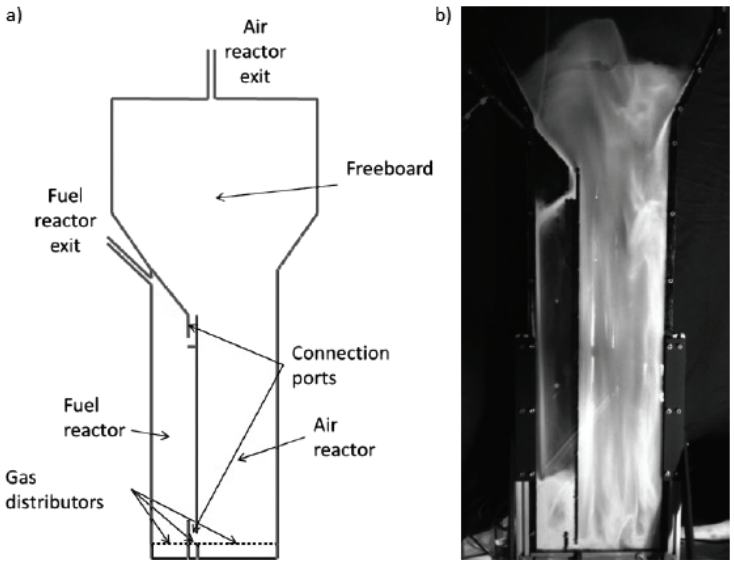

Figure 1: a) Simplified scheme of the pseudo-2D cold-flow ICR design and b) pseudo-2D cold-flow ICR unit under operation.

Nomenclature

α	Volume fraction
ϕ_{pq}	Energy dissipation through drag (W/m^3)
γ_{Θ}	Energy dissipation through collisions (W/m^3)
λ_p	Bulk viscosity (Pa.s)
μ	Viscosity (Pa.s)
Θ	Granular temperature (m^2/s^2)
ρ	Density (kg/m^3)
$\vec{\upsilon}$	Velocity vector (m/s)

∇	Gradient operator (1/m)
$\overline{\overline{\tau}}$	Stress tensor (kg/(m.s^2))
C_D	Drag coefficient
d_{gr}	Grain diameter (m)
d_p	Particle diameter (m)
F_D	Drag force coefficient (1/s)
$\vec{g}$	Gravity vector (m/s^2)
$\overline{I}$	Identity tensor
$\vec{J}$	Species diffusive flux (kg/(m^2.s))
K_{sg}	Interphase momentum exchange coefficient (kg/(m^3.s))
k	Reaction rate constant
M	Molar weight (kg/mol)
N	Number of moles (mol)
n	Reaction order
P	Pressure (bar)
p	Pressure (Pa)
R	Ideal gas constant (J/mol.K)
R^H	Heterogeneous reaction rate (mol/m^{3}s)
Re_p	Particle Reynolds number
$\overline{S}$	Strain rate (1/s)
T	Temperature (K)
t	Time (s)
V	Volume (m^3)
X	Conversion
Y	Mass fraction

Subscripts

g	Gas
i	Species index
q	Phase index
s	Solids

2. Reactor simulations

This paper presents reactive multiphase flow modelling simulations to estimate gas leakage between the sections of an ICR employed for chemical looping combustion. Two sets of simulations are presented: hydrodynamic simulations for quantifying the gas/solids leakage ratio through the two ports and reactive simulations for quantifying the amount of oxygen carrier conversion that can be achieved.

2.1. Model equations

Simulations were carried out using the dense discrete phase model (DDPM) where parcels of particles are tracked through the domain in a Lagrangian framework according to Newton's laws of motion. The DDPM extends the conventional discrete phase model (DPM) by also accounting for the volume fraction of the discrete phase [10].

The continuity and momentum equations for the gas are solved in the standard form:

$$\frac{\partial}{\partial t}\left(\alpha_g \rho_g\right) + \nabla \cdot \left(\alpha_g \rho_g \vec{\upsilon}_g\right) = 0 \tag{1}$$

$$\frac{\partial}{\partial t}\left(\alpha_g \rho_g \vec{\upsilon}_g\right) + \nabla \cdot \left(\alpha_g \rho_g \vec{\upsilon}_g \vec{\upsilon}_g\right) = -\alpha_g \nabla p + \nabla \cdot \overline{\overline{\tau}}_g + \alpha_g \rho_g \vec{g} + K_{sg}\left(\vec{\upsilon}_s - \vec{\upsilon}_g\right) \tag{2}$$

Inter-phase momentum exchange $\left(K_{sg}\right)$ was modelled according to the formulation of Syamlal and O'Brien [11].

Parcels of particles are tracked through the domain according to Newton's 2nd law:

$$\frac{d\vec{\upsilon}_p}{dt} = F_D\left(\vec{\upsilon} - \vec{\upsilon}_p\right) + \frac{\vec{g}\left(\rho_p - \rho\right)}{\rho_p} - \frac{\nabla p_s}{\alpha_p \rho_p} \tag{3}$$

The drag force coefficient $\left(F_D\right)$ was calculated from the drag coefficient proposed in Ref. [11]:

$$F_D = \frac{18\mu}{\rho_p d_p^2}\frac{C_D \operatorname{Re}_p}{24} \tag{4}$$

The final term in Equation (3) is a simplified model representation of the interaction between particles. It does not have the highest possible accuracy but favors efficiency, particularly when compared to DEM approaches. A major limitation of this formulation is that the particle interaction force does not contain any viscous contribution. The resistance to strain caused by the modelled shear viscosity is therefore not included.

The granular temperature used in the KTGF is calculated in its algebraic form from the ordinary differential equation below:

$$\frac{3}{2}\left[\frac{\partial}{\partial t}\left(\alpha_p \rho_p \Theta\right)\right] = \overline{\tau}_p : \nabla \vec{\upsilon}_p + \gamma_\Theta + \phi_{pq} \tag{5}$$

Here, the right hand side terms represent the generation of fluctuating energy by the solids stress tensor, the collisional dissipation of fluctuating energy [12] and the energy exchange between the fluctuating particles and any additional phases [13]. The solids stress tensor in Equation (5) is written as follows:

$$\overline{\tau}_p = -p_p \overline{I} + 2\mu_p \overline{S} + \left(\lambda_p - \frac{2}{3}\mu_p\right) \cdot \nabla \vec{\upsilon}_p \overline{I} \tag{6}$$

Here, the solids pressure and the bulk viscosity are calculated according to Lun *et al.* [12] and the shear viscosity according to Syamlal *et al.* [11]. Within these formulations, the radial distribution function is calculated according to Ogawa *et al.* [14].

When the particle volume fraction exceeds 75% of the volume fraction at maximum packing (0.63), a special treatment is applied to ensure numerical stability. In this treatment, the solids phase is convected by solving the Eulerian momentum equation and particle positions are updated accordingly.

$$\frac{\partial}{\partial t}\left(\alpha_g \rho_g \vec{\upsilon}_g\right) + \nabla \cdot \left(\alpha_g \rho_g \vec{\upsilon}_g \vec{\upsilon}_g\right) = -\alpha_s \nabla p - \nabla p_s + \nabla \cdot \overline{\overline{\tau}}_s + \alpha_s \rho_s \vec{g} + K_{gs}\left(\vec{\upsilon}_g - \vec{\upsilon}_s\right) \tag{7}$$

2.2. Reaction kinetics

Reactive simulations included in this study simulated chemical looping combustion reactions of syngas over ilmenite. The following simplified reactions were included:

$$H_2 + Fe_2O_3 \rightarrow 2FeO + H_2O$$
$$CO + Fe_2O_3 \rightarrow 2FeO + CO_2$$
$$O_2 + 4FeO \rightarrow 2Fe_2O_3$$

Species were conserved as follows:

$$\frac{\partial}{\partial t}\left(\alpha_q \rho_q Y_{q,i}\right) + \nabla \cdot \left(\alpha_q \rho_q \vec{\upsilon}_q Y_{q,i}\right) = \nabla \cdot \alpha_q \vec{J}_{q,i} + \alpha_q S_{q,i} \tag{8}$$

The source term on the right of Equation (8) is due to heterogeneous reactions. The following reaction rate expression was used:

$$R_i^H = -\frac{1}{V}\frac{dN_i}{dt} = \frac{6}{d_{gr}}\left(1-X\right)^{2/3} \alpha_s k \left(\frac{Y_i \rho_g}{M_i}\right)^n \tag{9}$$

The grain diameter $\left(d_{gr}\right)$ is 2.5 µm and the reaction orders $\left(n\right)$ are 1 for reactions involving H_2 and O_2, and 0.8 for reduction with CO [15]. The reaction rate constants $\left(k\right)$ for different reactions are taken from Abad et al. [15] with the addition of an inverse proportionality to pressure as observed in Ref. [16].

$$k_{H_2} = \frac{0.062}{P^{0.8}} e^{\left(\frac{-65000}{RT}\right)}$$
$$k_{CO} = \frac{0.1}{P^{0.8}} e^{\left(\frac{-80700}{RT}\right)} \tag{10}$$
$$k_{O_2} = \frac{0.0019}{P^{0.8}} e^{\left(\frac{-25500}{RT}\right)}$$

No energy conservation was included in the reactive simulations because the heat balance complicated the assessment of the degree of conversion of the oxygen carrier that could be achieved before fuel slip takes place. As described later, this was conveniently assessed while maintaining hydrodynamic similarity by changing the mole fraction of combustible gases entering fuel section of the ICR. This would influence the reactor heat balance and complicate the simulation campaign if energy conservation is included. For the purpose of the current exploratory study, this is a reasonable simplifying practice, but energy conservation should definitely be included if the DDPM is used to aid in ICR design.

2.3. Geometry, materials and boundary conditions

The simulated geometry is displayed in Figure 2. The height of the simulated reactor is 20 m with a 4x4 m^2 cross sectional area. The two reactor sections have an equal cross sectional area and are separated by a vertical partition rising to a height of 10 m, followed by a diagonal partition positioned at a 45° angle. The top port is 0.4x0.4 m^2 in cross sectional area and extends 4 m down from the diagonal partition (down to a reactor height of 6 m), while the

bottom port is only 1 m high with a cross sectional area of 0.2x0.2 m^2. Simulation experience showed that the top port should be larger than the bottom port to allow a sufficient amount of particles to fall into the port in order to circulate to the other reactor section. Both ports are open at the top and have a 0.2x0.2 m^2 opening at the bottom oriented parallel to the central partition.

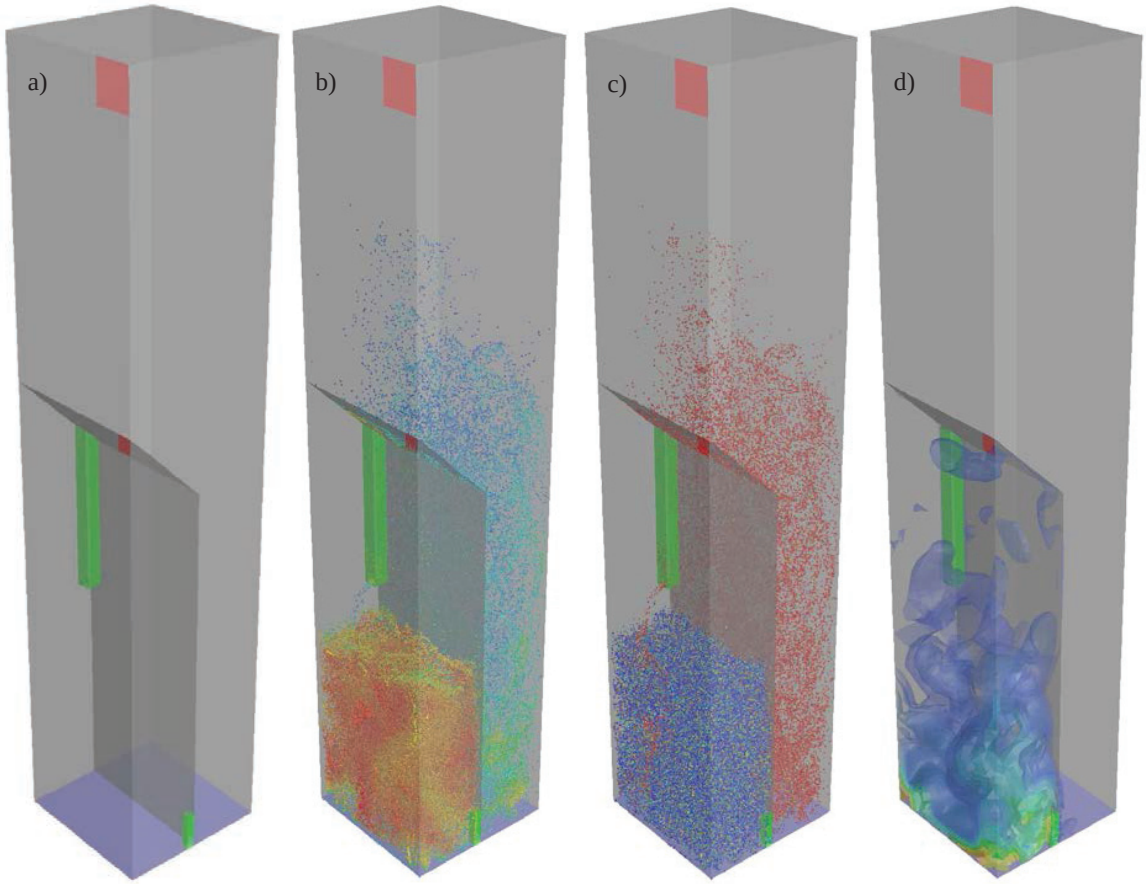

Figure 2: The simulated ICR geometry (a) with the inlets coloured blue, the outlets coloured red and the connecting ports coloured green. The two central images show the DPM parcels being tracked by the DDPM approach. In (b) the parcels are coloured by solids volume fraction and in (c) by the oxidized oxygen carrier species (Fe_2O_3) mass fraction on a blue-green-red colour scale. Image (d) shows iso-surfaces of the CO mole fraction illustrating fuel slip on a blue-green-red colour scale.

The geometry was meshed with 43000 hexahedral cells with a targeted cell size of 0.2x0.2x0.2 m^3. One level of hanging node refinement was completed in the ports, dividing each cell into 8 approximately equally sized cells.

A density of 4000 kg/m^3 and a particle size of 200 µm was selected for the ilmenite oxygen carrier. 153.6 tons of this material was injected into the reactor (enough to create a 4 m static bed in both reactor sections). For the non-reactive simulations, the gas density was assumed to be 4.5 kg/m^3 and the viscosity as 4.5e-5 Pa.s. Two gas species with identical properties were fed to the two different reactor sections in order to study the gas leakage. Gas was injected at 2 m/s in the fast section (back-right in Figure 1a) and 0.2 m/s in the slow section (front-left in Figure 1a).

For the reactive simulations, the ideal gas law was employed for the density and the kinetic theory for the viscosity at a reactor temperature and pressure of 900 °C and 20 bar respectively. Air was fed to the fast section and syngas to the slow section according to Table 1. These feed conditions approximate a chemical looping combustion ICR with a capacity of approximately 100 MW_{th}.

Table 1: Inlet conditions to the reactive ICR simulations.

Stream	Mass flow (kg/s)	Composition (mole fraction)	
Fast section (oxidation)	100	O_2	0.21
		N_2	0.79
Slow section (reduction)	10	H_2	0.23
		CO	0.57
		H_2O	0.09
		CO_2	0.11

2.4. Solver settings

The commercial CFD package, FLUENT 16.1 was used as the flow solver to carry out the simulations. The phase-coupled SIMPLE algorithm [17] was selected for pressure-velocity coupling, while the QUICK scheme [18] was employed for discretization of all remaining equations. 2nd order implicit temporal discretization was used.

3. Results and discussion

Three sections of results follow below. Firstly, the hydrodynamic simulation results will be presented to assess the gas leakage performance of the ICR. Secondly, the relationship between the degree of oxygen carrier utilization (average degree of reduction in the fuel reactor) and fuel slip will be investigated via reactive simulations. And finally, these simulation results will be employed to complete simplified mass balance calculations estimating the CO_2 separation performance of four different chemical looping applications: combustion, reforming, oxygen production and water splitting.

3.1. Hydrodynamic simulations

It is important to understand the hydrodynamic behavior of the ICR in order to ensure a sufficient solids circulation rate and minimize gas leakage. In order to ensure good circulation, the particles in the fast section must rise significantly above the upper end of the top port in Figure 2 in order to enter the port and circulate to the slow section. At the same time, the pressure at the bottom of the slow section must be substantially higher than at the bottom of the fast section in order to drive particles through the bottom port, implying that the bed in the slow section must be much denser than in the fast section (see Figure 2b). In addition, it was experimentally determined that the leakage through the top port could be reduced substantially by applying a slight overpressure in the slow section of the reactor [9].

This mechanism will be investigated in more detail in this section by applying various overpressures to the slow section and monitoring the gas leakage performance of the reactor. As illustrated in Figure 3, the gas/solids leakage ratio through the top (fast-to-slow) port reduces substantially with an increase in the overpressure on the slow reactor side. A higher pressure in the slow section reduces the driving force for gas to leak from the fast to the slow section and can also result in a solids plug forming in the top port, restricting gas flow.

The graph also shows the percentage of leaked gas to and from the slow section. These measures are indicative of CO_2 purity and capture efficiency respectively. As expected, the trends of gas leakage closely reflect the gas/solids leakage ratio trends. A slight improvement in leakage performance relative to the gas/solids leakage ratio can be observed with an increase in slow section overpressure. This is due to the solid circulation rate reducing from about 260 kg/s at 0 kPa overpressure to 200 kg/s at 30 kPa overpressure.

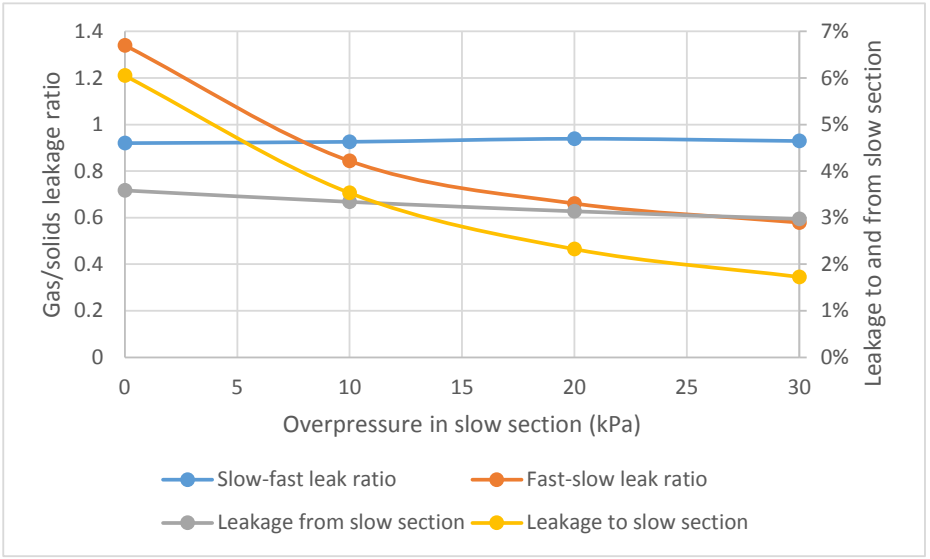

Figure 3: Gas leakage performance of the ICR as a function of overpressure in the slow section.

The positive effect of overpressure in the slow section is clear from Figure 3, but it is not possible to extend this effect indefinitely. In fact, an overpressure of 40 kPa and above resulted in a situation where the top port is blown clear of all particles by a gas stream passing from the slow to the fast section. This constant gas stream prevents any particles from falling into the top port and blocking the passage of gas, thus preventing any solids circulation through the top port. Overpressure in the slow section of the reactor can therefore prevent proper reactor functionality if pushed too high.

3.2. Reactive simulations

Minimizing the solids circulation rate in an ICR helps to minimize leakage of gas with the solids moving through the ports. If the solids circulation rate is reduced too much, however, insufficient oxidized material will be available in the fuel reactor, leading to fuel slip (see Figure 2d). The concentrated addition of material from the top port could also lead to a non-uniform distribution of oxidized material in the fuel section, further enhancing fuel slip. It is therefore important to quantify the amount of fuel slip taking place as a function of solids circulation rate.

Figure 4 illustrates this effect as a function of the degree of oxygen carrier utilization at complete fuel conversion. The maximum amount of fuel (H_2 and CO) that could be combusted by the oxidized oxygen carrier circulating at a mass flow rate of 253 kg/s was calculated to be 523 mol/s for the ilmenite oxygen carrier used in this study – significantly more than the 350 mol/s entering in the base case (Table 1). The amount of H_2 and CO in the incoming syngas was then set to 100%, 80% (base case), 60% and 40% while keeping the H_2:CO ratio and incoming molar flowrate constant. This strategy kept the hydrodynamic behavior of the ICR approximately constant between different cases in order to isolate the effect of oxygen carrier utilization on fuel slip and simplify/shorten the simulation campaign.

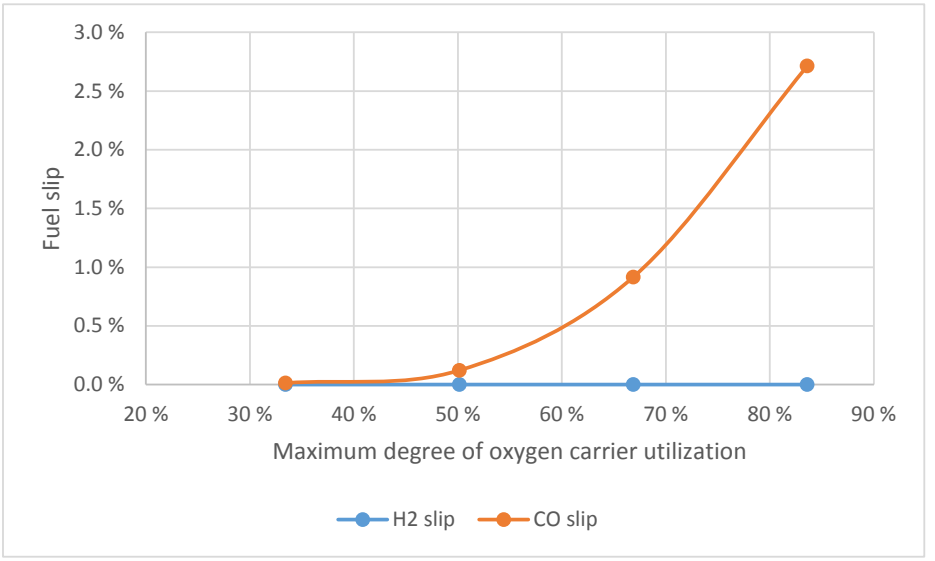

Figure 4: Fuel slip as a function of the degree of oxygen carrier utilization at complete fuel conversion.

As illustrated in Figure 4, fuel slip is insignificant (<0.1%) at an oxygen carrier utilization of up to 50%. It is also clear that only CO slip is significant due to the much higher reactivity of H_2. Fuel slip increases significantly with oxygen carrier utilization because the reaction rate decreases with the degree of oxygen carrier reduction. In addition, fuel slip is slightly enhanced by the uneven distribution of reactive species in the fuel section (see Figure 2c), but the reactor approximates the behavior of a continuously stirred tank reactor (CSTR) quite well.

In addition, the CO_2 purity and capture efficiency could be directly quantified in this case as 96% and 97% respectively for the base case. A 20 kPa overpressure was applied in the fuel section to limit gas leakage through the top port, thus enhancing CO_2 purity.

3.3. CO_2 separation performance of different chemical looping technologies

The central variable in this analysis will be the gas/solids leakage ratio (the ratio of volumetric gas and solids flow through the ports). As illustrated via the hydrodynamic simulations, a gas solids leakage ratio of about 0.94 and 0.66 can be achieved through the bottom and top ports respectively in the case with 20% overpressure in the slow section (Figure 3). This information will be used to estimate the CO_2 separation performance in the ICR as applied to different chemical looping concepts.

As illustrated in Ref. [9], the basic methodology starts with calculating the amount of fuel that can be fed to the reactor assuming an oxygen carrier circulation rate of 1 kg/s. Subsequently, the gas leakage between reactor sections associated with this 1 kg/s solids circulation rate is expressed as a function of the gas/solids leakage ratio. The CO_2 purity can then simply be calculated as the ratio between the depleted air leaking from the oxidation section and the total amount of CO_2 formed in the reduction section. Similarly, CO_2 capture can be calculated as the ratio between the CO_2 leaking from the reduction section and the total amount of CO_2 formed in the reduction section.

The most important parameters and results from these calculations are outlined in Table 2. Combustion of syngas over ilmenite is carried out using 50% oxygen carrier utilization to avoid fuel slip as derived from the reactive simulations presented earlier. The reforming application is assumed to proceed with hydrogen perm-selective membranes extracting all the hydrogen that can be formed through reforming when 30% of the incoming fuel is combusted to provide heat for the endothermic reforming reaction. Operating conditions for this application are taken from Ref. [19]. Oxygen production is carried out as integrated into an IGCC power cycle as outlined in Ref. [20]. The unit produces about 17% O2 in a stream of CO_2 and H_2O for feeding to the gasifier. 50% of the released oxygen reacts with the incoming fuel to achieve the desired reactor temperature, while the remaining 50% exits in

the N_2-free stream to the gasifier. Water splitting is carried out via the well-known steam-iron process according to conditions outlined in Ref. [21].

Table 2: Parameters used in the CO_2 separation efficiency estimates for different chemical looping applications of the ICR concept. The fuel feed rate and gas leakage (last two rows) are calculated based on a solids circulation rate of 1 kg/s.

Parameter	Combustion	Reforming	Oxygen production	Water splitting
Oxygen carrier	Ilmenite	Nickel oxide	CAM	Iron oxide
Oxidized active species	Fe_2O_3	NiO	$Ca_2AlMnO_{5.5}$	Fe_2O_3
Active species content	33%	40%	100%	30%
Degree of conversion	50%	80%	100%	80%
Material density (kg/m^3)	4250	3400	2500	3500
Temperature (K)	1400	1000	1100	1100
Pressure (bar)	20	50	20	20
CO_2 in combusted fuel	68%	58%	72%	33%
Fuel feed rate (mol/s)	**1.03**	**3.57**	**2.34**	**0.38**
Leakage at gas/solids leak ratio of 1 (mol/s)	**0.041**	**0.179**	**0.088**	**0.063**

Good CO_2 separation performance will be achieved when a large amount of fuel can be processed from the fixed solids circulation rate of 1 kg/s (second-last row in Table 2). It is clear that the reforming and oxygen production will do the best in this regard. This is because only 30% and 50% of the incoming fuel is combusted in these respective processes. The reforming application also benefits from the high oxygen transport capacity of NiO oxygen carriers. Water splitting fares the worst in this category because the fuel reactor (combustor) receives only partially oxidized oxygen carrier (50% Fe_2O_3 and 50% Fe_3O_4) and the fuel is methane (a low flowrate is required by stoichiometry).

In addition, low gas leakage through the ports must be achieved to ensure good CO_2 separation (last row in Table 2). In this case, the reforming application performs the worst due to the high system pressure (50 bar). The combustion application performs best due to the dense oxygen carrier and the high operating temperature (which reduces the gas density). When combining these factors to calculate the CO_2 purity and capture for each application, the trends in Figure 5 emerge.

It is clear that the oxygen production process performs best, followed by the reforming and combustion applications. The water splitting application achieves poor CO_2 separation performance due to the high oxygen carrier circulation rate required.

The trend for CO_2 purity is generally worse than for CO_2 capture. This is due to the combusted gases containing some steam which is condensed out before CO_2 compression. The leaked N_2 from the oxidation reactor section therefore represents a larger fraction of the CO_2 for compression than the total combusted gases exiting the reduction reactor section. This is especially severe for the water splitting application where pure methane is combusted, yielding one part CO_2 in two parts steam. The reforming application is also fed with methane, but the membranes extract a large portion of the produced steam as hydrogen (produced by the water-gas shift reaction), yielding a higher CO_2 content in the exiting gases.

As shown by the reactor simulations discussed in previous sections, leakage through the top port (which will generally affect the CO_2 purity) can be significantly lower than leakage through the bottom port (which will generally affect the CO_2 capture). This effect will compensate for the difficulty of achieving high CO_2 purities described above. When assuming the gas/solids leakage ratios returned by the reactor simulations (0.66 through the top port and 0.94 through the bottom port), the following CO_2 separation performance is achieved:

- Combustion: 96.3% purity and 96.3% capture
- Reforming: 96.8% purity and 97.3% capture
- Oxygen production: 97.6% purity and 97.4% capture
- Water splitting: 90.0% purity and 94.8% capture

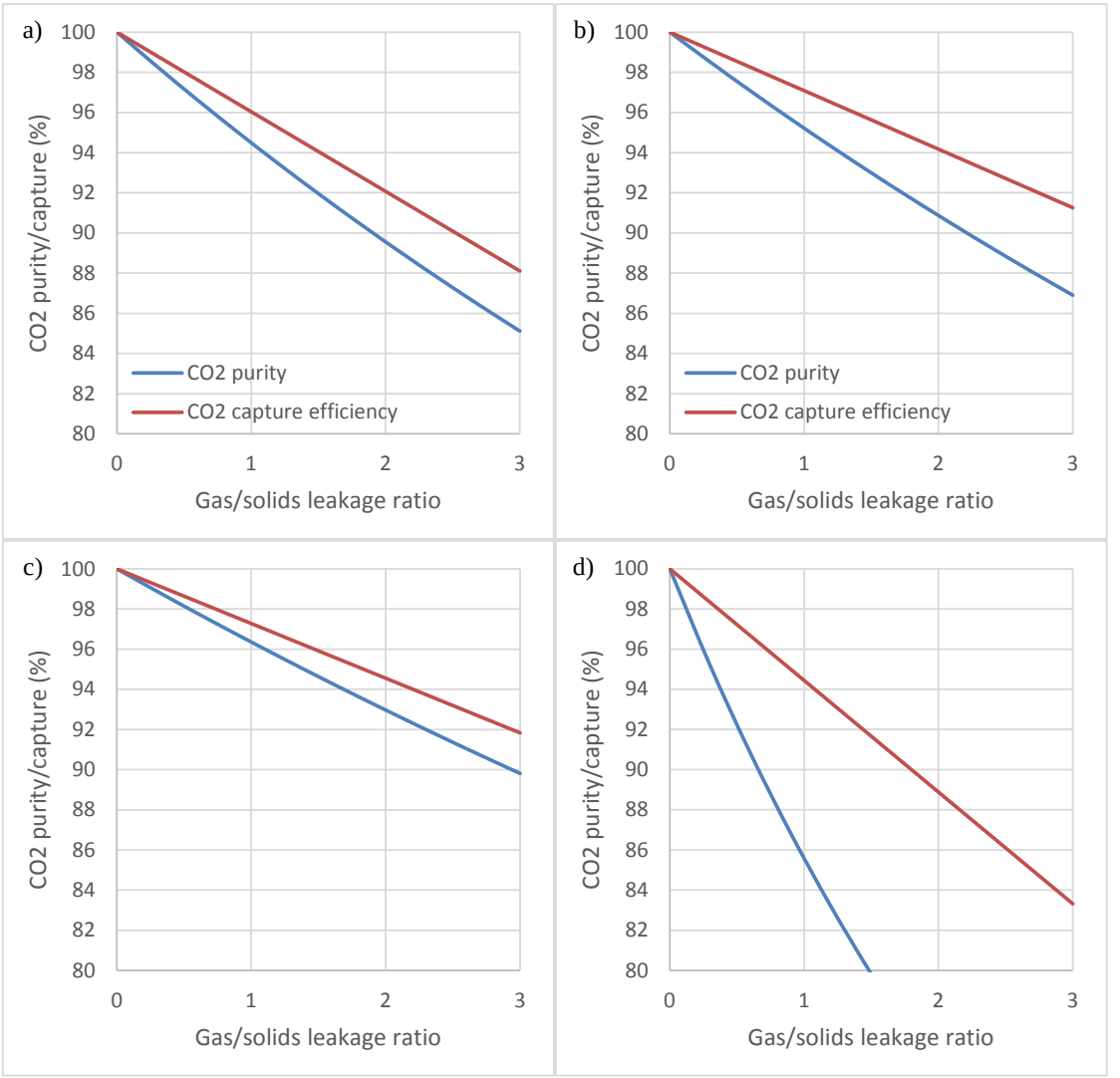

Figure 5: CO_2 purity and capture as a function of gas/solids leakage ratio for a) combustion, b) reforming, c) oxygen production and d) water splitting applications of chemical looping carried out in the ICR.

4. Conclusions

The internally circulating reactor (ICR) is a promising new concept for simplified scale-up of pressurized chemical looping technologies. Cyclones and loop seals from the conventional dual circulating fluidized bed concept are replaced by two simple ports and the entire reactor can be designed as a single pressure vessel.

Cold flow experiments have shown that reliable solids circulation can be achieved in an ICR and reactive multiphase flow modelling has extended this conclusion to a large-scale (100 MW_{th}) reactor. The key challenge of undesired gas leakage with the circulating solids was investigated in more detail in this study. It was shown that low gas leakage rates can be achieved, especially through the top port of the ICR reactor by applying some overpressure in the slow (fuel) section of the reactor. Reactive simulations showed good CO_2 purity and capture of 96% and 97% respectively for the chemical looping combustion application of ICR.

Using insights from reactive multiphase flow modelling, the CO_2 separation performance of the ICR applied to chemical looping applications of combustion, reforming, oxygen production and water splitting was estimated. Very good CO_2 separation performance was achieved by the oxygen production application (~97.5% CO_2 purity and capture) as well as the combustion and reforming applications (>96% CO_2 purity and capture). CO_2 separation performance in the water splitting application was lower (CO_2 purity of only 90%), implying that the ICR is not such an attractive solution unless steam purging is applied in the ports between the reactor sections. For the other applications, the ICR appears to be an attractive technology for accelerating scale-up of these promising clean energy technologies.

Acknowledgements

The authors gratefully acknowledge the financial support from the Research Council of Norway under the ICR project (project number: 255462).

References

[1] M. Ishida, D. Zheng, T. Akehata, Evaluation of a chemical-looping-combustion power-generation system by graphic exergy analysis, Energy, 12 (1987) 147-154.
[2] A. Lyngfelt, B. Leckner, T. Mattisson, A fluidized-bed combustion process with inherent CO2 separation; Application of chemical-looping combustion, Chem. Eng. Sci., 56 (2001) 3101-3113.
[3] M. Ryden, A. Lyngfelt, T. Mattisson, Two novel approaches for hydrogen production; chemical-looping reforming and steam reforming with carbon dioxide capture by chemical-looping combustion, in: 16th World Hydrogen Energy Conference 2006, WHEC 2006, June 13, 2006 - June 16, 2006, Association Francaise pour l'Hydrogene et les Piles a, Lyon, France, 2006, pp. 703-710.
[4] B. Moghtaderi, Application of Chemical Looping Concept for Air Separation at High Temperatures, Energy & Fuels, 24 (2010) 190-198.
[5] M. Rydén, M. Arjmand, Continuous hydrogen production via the steam–iron reaction by chemical looping in a circulating fluidized-bed reactor, International Journal of Hydrogen Energy, 37 (2012) 4843-4854.
[6] R. Xiao, L. Chen, C. Saha, S. Zhang, S. Bhattacharya, Pressurized chemical-looping combustion of coal using an iron ore as oxygen carrier in a pilot-scale unit, International Journal of Greenhouse Gas Control, 10 (2012) 363-373.
[7] S. Noorman, M. van Sint Annaland, Kuipers, Packed Bed Reactor Technology for Chemical-Looping Combustion, Industrial & Engineering Chemistry Research, 46 (2007) 4212-4220.
[8] A. Zaabout, S. Cloete, S.T. Johansen, M. van Sint Annaland, F. Gallucci, S. Amini, Experimental Demonstration of a Novel Gas Switching Combustion Reactor for Power Production with Integrated CO2 Capture, Industrial & Engineering Chemistry Research, 52 (2013) 14241-14250.
[9] A. Zaabout, S. Cloete, S. Amini, Innovative Internally Circulating Reactor Concept for Chemical Looping-Based CO2 Capture Processes: Hydrodynamic Investigation, Chemical Engineering & Technology, 39 (2016) 1413-1424.
[10] B. Popoff, M. Braun, A Lagrangian Approach to Dense Particulate Flows, in: 6th International Conference on Multiphase Flow, Leipzig, Germany, 2007.
[11] M. Syamlal, W. Rogers, T.J. O'Brien, MFIX Documentation: Volume 1, Theory Guide., National Technical Information Service, Springfield, 1993.
[12] C.K.K. Lun, S.B. Savage, D.J. Jeffrey, N. Chepurniy, Kinetic Theories for Granular Flow: Inelastic Particles in Couette Flow and Slightly Inelastic Particles in a General Flow Field, Journal of Fluid Mechanics, 140 (1984) 223-256.
[13] D. Gidaspow, R. Bezburuah, J. Ding, Hydrodynamics of Circulating Fluidized Beds, Kinetic Theory Approach, in: 7th Engineering Foundation Conference on Fluidization 1992, pp. 75-82.
[14] S. Ogawa, A. Unemura, N. Oshima, On the Equation of Fully Fluidized Granular Materials, Journal of Applied Mathematics and Physics, 31 (1980) 483.
[15] A. Abad, J. Adánez, A. Cuadrat, F. García-Labiano, P. Gayán, L.F. de Diego, Kinetics of redox reactions of ilmenite for chemical-looping combustion, Chem. Eng. Sci., 66 (2011) 689-702.
[16] F. García-Labiano, J. Adánez, L.F. de Diego, P. Gayán, A. Abad, Effect of Pressure on the Behavior of Copper-, Iron-, and Nickel-Based Oxygen Carriers for Chemical-Looping Combustion, Energy & Fuels, 20 (2005) 26-33.
[17] S. Patankar, Numerical Heat Transfer and Fluid Flow, Hemisphere Publishing Corporation, United States, 1980.
[18] B.P. Leonard, S. Mokhtari, ULTRA-SHARP Nonoscillatory Convection Schemes for High-Speed Steady Multidimensional Flow, in: NASA TM 1-2568 (ICOMP-90-12), NASA Lewis Research Center, 1990.
[19] V. Spallina, D. Pandolfo, A. Battistella, M.C. Romano, M. Van Sint Annaland, F. Gallucci, Techno-economic assessment of membrane assisted fluidized bed reactors for pure H2 production with CO2 capture, Energy Conversion and Management, 120 (2016) 257-273.
[20] Y. Larring, S. Cloete, A. Giuffrida, M. Romano, P. Chiesa, J. Morud, M. Pishahang, A. Chikukwa, S. Amini, A. Tobiesen, COMPOSITE: A concept for high efficiency power production with integrated CO2 capture from solid fuels, in: 13th International Conference on Greenhouse Gas Control Technologies, Lausanne, Switzerland, 2016.
[21] D. Sanfilippo, One-step hydrogen through water splitting with intrinsic CO2 capture in chemical looping, Catalysis Today, 272 (2016) 58-68.